Analytical model of foreshock ion interaction with a discontinuity: a statistical study

Terry Z. Liu[1], Andrew Vu[1], Vassilis Angelopoulos[1], and Hui Zhang[2]

[1]Department of Earth, Planetary, and Space Sciences, University of California, Los Angeles, USA. [2]Geophysical Institute, University of Alaska Fairbanks, USA

Key points

1. We derive a model that describes foreshock ion – discontinuity interaction, which is consistent with local hybrid simulations.
2. We obtain moderate correlations between the model expansion speed and (a) magnetic field variations, and (b) dynamic pressure depletions.
3. Our model can potentially predict strong dynamic pressure depletion caused by foreshock ion-discontinuity interaction.

Abstract

When a solar wind discontinuity interacts with foreshock ions, foreshock transients such as hot flow anomalies and foreshock bubbles can form. These create significant dynamic pressure perturbations disturbing the bow shock, magnetopause, and magnetosphere-ionosphere system. However, presently these phenomena are not predictable. In the accompanying paper, we derived analytical equations of foreshock ion partial gyration around a discontinuity and the resultant current density. In this study, we utilize the derived current density strength to model the energy conversion from the foreshock ions, which drives the outward motion or expansion of the solar wind plasma away from the discontinuity. We show that the model expansion speeds match those from local hybrid simulations for varying foreshock ion parameters. Using MMS, we conduct a statistical study showing that the model expansion speeds are moderately correlated with the magnetic field strength variations and the dynamic pressure decreases around discontinuities with correlation coefficients larger than 0.5. We use conjunctions between ARTEMIS and MMS to show that the model expansion speeds are typically large for those already-formed foreshock transients. Our results show that our model can be reasonably successful in predicting significant dynamic pressure disturbances caused by foreshock ion-discontinuity interactions. We discuss ways to improve the model in the future.

1. Introduction

When foreshock ions interact with a solar wind discontinuity, a hot flow anomaly (HFA) (e.g., Schwartz et al., 1985, 2018; Lin, 1997, 2002; Omidi and Sibeck, 2007; Zhang et al., 2010) or a foreshock bubble (FB) (e.g., Omidi et al., 2010, 2020; Turner et al., 2013, 2020; Liu et al., 2015; Wang C.-P. et al., 2021a, b) may form. These foreshock transients are characterized by a core region with field strength decrease, density decrease, temperature increase, and flow deflection, on a spatial scale of a few R_E (see review by Eastwood et al. (2005), Facskó et al. (2010), and Zhang et al. (2022)). Because the dynamic pressure inside them is extremely low, they can cause the local bow shock and magnetopause to move outward, leading to disturbances in the magnetosphere and ionosphere, including magnetospheric ULF waves, field aligned currents, traveling convection vortices, and auroral brightening (e.g., Sibeck et al., 1999; Eastwood et al., 2011; Fillingim et al., 2011; Hartinger et al., 2013; Archer et al., 2014, 2015; Shi et al., 2013, 2017; Zhao et al., 2017; Wang B. et al., 2019, 2020, 2021; Shen et al., 2018; Shi et al., 2020; Liu et al., 2022a), from dayside to far tail (Facskó et al., 2015; Wang C.-P. et al., 2018, 2020, 2021b; Liu et al., 2020a, 2021).

However, these foreshock phenomena and the associated magnetosphere-ionosphere disturbances are not yet predictable. Contrary to the solar wind potential drivers of magnetospheric activity (e.g., interplanetary shocks) that can be predicted and monitored in advance, foreshock transients cannot, partly because they are rather localized near the bow shock and have been hard to recognize, identify, and study with previous single spacecraft missions. The situation has improved drastically with the advent of Cluster, THEMIS, and MMS missions. It has been possible to confirm many expectations from simulations, such as the scale-size, evolution, and other characteristics of foreshock transients (e.g., Lucek et al., 2004; Facskó et al., 2009, 2010; Liu et al., 2016; Lee et al., 2021), as well as the physical mechanism leading to their formation, namely the interaction of the foreshock ions with the approaching discontinuity (Liu et al., 2020b). Given this level of physical understanding, one is tempted to take the next step to formulate a predictive model of a transient's formation and impacts based on pristine upstream solar wind conditions. Based on previous simulations (e.g., Thomas et al, 1991; Lin, 2002; Omidi and Sibeck, 2007; Omidi et al., 2010; Wang C.-P. et al., 2021b), it is commonly thought that the concentration and thermalization of foreshock ions at a discontinuity increases the local thermal pressure causing the formation and expansion of an HFA or FB. However, this understanding is too qualitative and cannot be used to model the formation process.

Recently, a kinetic model has been proposed based on PIC simulations (An et al., 2020) and MMS observations (Liu et al., 2020b). When foreshock ions encounter a solar wind discontinuity, as their gyroradii are comparable to the discontinuity thickness, they perform partial gyration. In the accompanying paper (Liu et al., 2022 submitted to JGR), we derived the analytical equations of foreshock ion motion across a discontinuity. Because electrons are magnetized, the motion difference between the foreshock ions and electrons leads to a current. If this current tends to decrease the field strengths at the discontinuity, more foreshock ions can cross the discontinuity which strengthen the current resulting in positive feedback. The magnetic field variation by the current induces an electric field, which drives cold plasma to E×B drift outward away from the discontinuity, i.e., the expansion process. The energy conversion to the expansion energy of solar wind plasma is through the foreshock ion current against the induced electric field. Such a formation and expansion process has been further examined by local hybrid simulations by Vu et al. (2022a). Based on the energy conversion, Liu et al. (2023) derived an expansion speed model. These modeling successes show that it has become increasingly possible to quantitatively describe the formation and expansion process of foreshock transients.

In this study, we take yet another step in the quantitative description of foreshock transients and their effects by combining the foreshock ion motion model (Liu et al., 2022 submitted to JGR) and the expansion speed model (Liu et al., 2023) to quantitatively describe the expansion speed of the transient due to the foreshock ion – discontinuity interaction. This model describes the early interaction between the foreshock ions and a discontinuity, which generates small perturbations that may or may not evolve into an FB, an HFA, or a structure that belongs to neither. We test how well it works by comparing with local hybrid simulations and observations. In Section 2, we introduce the model and compare it with local hybrid simulations. In Section 3, we introduce the database and describe how we conduct a statistical study and case studies to test the model. The results are presented in Section 4 and summarized in Section 5.

2. Model description

The expansion speed model by Liu et al. (2023) showed that the foreshock ions transfer energy to the solar wind plasma through the current density driven by the foreshock ions j against the induced electric field E in the solar wind rest frame. The solar wind plasma gains energy and moves away from the discontinuity at a speed $E \times B$, i.e., the expansion of the transient. The expansion speed can be expressed as

$$V_{exp} = j/qn_{sw} \cdot \Omega_i \Delta t \quad (1),$$

where q is the unit charge, n_{sw} is solar wind density, and Ω_i is ion gyrofrequency. Based on local hybrid simulations by Vu et al., (2023), $\Omega_i \Delta t$ in Eq. (1) should be modified as $(\Omega_i \Delta t)^2$, due to the positive feedback from the field variation which can further enhance the current. However, in observations it is nearly impossible to determine how long the structure has been evolving. Thus, we do not include the time dependence in this study and simplify Eq. (1) as $V_{exp} = \pi j/qn_{sw}$ to represent a typical expansion speed for each observation event.

In the accompanying paper (Liu et al., 2022 submitted to JGR), we have derived that

$$j(x) \sim qn_f \left(\frac{1}{\pi v_{th\perp}^2}\right) \int_0^\infty \exp\left(-\frac{(V_\perp)^2}{v_{th\perp}^2}\right)\left(-V_\perp \Delta \sin\varphi_c \cos\alpha(x) + (V_{\parallel 0} - C)\sin\alpha(x)\,\Delta\varphi_c\right) V_\perp dV_\perp \quad (2),$$

assuming that foreshock ions follow Maxwellian distributions, where n_f is foreshock ion density, φ_c is the initial gyrophase of foreshock ions that can reach position *x* within a discontinuity along the normal direction, α is the shear angle of discontinuity, parameter $C = \Omega_i \frac{dx}{d\alpha}$, and for easy application in observations, we simplify that the foreshock ions approximately follow Maxwellian distributions. When $j(x) < 0$, the field strength decreases at the discontinuity, which favors further growth of the transient structure. Thus, for each observation event when the negative peak of $j(x)$ is stronger than the positive peak, we substitute the maximum of $|j(x)|$, j_{max}, into simplified Eq. (1) and have

$$V_{exp} = \pi j_{max}/qn_{sw} \quad (3).$$

We thus obtain a model that can predict the expansion speed of foreshock transients due to the interaction of the foreshock ions with the discontinuity, given the foreshock ion parameters (thermal speed, parallel speed, and density), solar wind density, interplanetary magnetic field (IMF) strength, and discontinuity parameters (shear angle and thickness).

To test this model, we first use the local hybrid simulation results by Vu et al. (2023). In the simulations, foreshock ions are injected from the simulation boundary (which acts as a bow shock) and interact with a tangential discontinuity (TD) with shear angle of 90°, forming an FB. The FB expansion speed was measured at a fixed distance from the "bow shock" and fixed time after the FB's initial formation. We scanned the parameter space of foreshock ion density, thermal speed, and parallel speed by varying each parameter while fixing others (TD shear angle and thickness, however, still need further tests). We transform the simulation parameters to the solar wind rest frame in which the model was derived and put them into the model. Figure 1 compares the model expansion speeds using Eq. (3) and the simulated expansion speeds. We see that they are linearly correlated, although the slope does not match the diagonal because the time dependence of the model is simplified, so the slope is determined by when the expansion speeds are measured in the simulations. Therefore, our model indeed captures the major physics.

Note that for varying foreshock ion parallel speed $V_{\|}$, we need to time a term $V_{\|0}/V_{\|}$ to the simulated expansion speed to match the model, where $V_{\|0}$ is the fixed foreshock ion parallel speed when the foreshock ion thermal speed and density are varied. This is because due to the simulation setup, the transient forms simultaneously while the foreshock ions are injected from the simulation boundary. The top of the structure is determined by how far the foreshock ions have reached upstream and the bottom is the simulation boundary or the "bow shock". The expansion speed spatially increases from 0 at the top to maximum at the bottom. At a fixed position in the simulation box where the expansion speed is measured, the distance to the structure top is $V_{\|}\Delta t$. We thus use term $V_{\|0}\Delta t/V_{\|}\Delta t$ to scale all the measured position to be the same relative to the transient structure.

As discussed above, the expansion speed is a function of both time and space, but in observations it is impossible to determine when and where the expansion speed is measured. So, the simplified model only provides a characteristic expansion speed for each observation event. Therefore, it is expected that the statistical results would be very scattered, but as shown in Section 4 our model is still good enough to show a moderate correlation with the observations.

This model describes the general foreshock perturbations due to foreshock ions interacting with a discontinuity. Because it is not a self-consistent model, i.e., the feedback of the magnetic field variations to the foreshock ion-driven current is not included, this model can only describe the early interaction before the magnetic field profile is significantly disturbed. Depending on how significant the expansion speed is, the configuration of the foreshock ion-driven currents, and other possible factors, the foreshock perturbations due to this early interaction may or may not evolve into an HFA, an FB, or a structure that does not satisfy the criteria of either of them. But as shown later, if our model can directly predict the magnetic field disturbances and dynamic pressure disturbances, it is not necessary to distinguish what phenomena they will become, especially because the physical differences between HFAs and FBs are still a puzzle and beyond the scope of this study.

3. Data and Methods

For the statistical study of foreshock ion-discontinuity interaction, we use the Magnetospheric Multiscale (MMS) mission (Burch et al., 2016) to observe discontinuities in the foreshock. We analyze DC magnetic field data from the fluxgate magnetometer (Russell et al., 2016) and plasma data from the fast plasma investigation (FPI) instrument suite (Pollock et al., 2016). We use time intervals when MMS is upstream of the bow shock from 2015 to 2019 identified by Vu et al. (2022b).

To automatically identify discontinuities, we calculate the magnitude of magnetic field vector change across 10 seconds normalized to its 4 min average; the resultant quantity, termed the normalized partial variance of increments (PVI) (e.g., Greco et al., 2008), $|\boldsymbol{B}(t+10s)-\boldsymbol{B}(t)|^2/\langle|\boldsymbol{B}(t+10s)-\boldsymbol{B}(t)|^2\rangle_{4\,min}$, is shown in Figure 2b. For each PVI > 5, i.e., there is a large magnetic field vector variation across 10 seconds relative to the 4 min average, we use 30s averaged magnetic field before and after as the background magnetic field and require the shear angle to be larger than 25°. Events with smaller shear angles are often contaminated by local fluctuations (especially steepened foreshock ULF waves) and therefore excluded. The discontinuity normal is calculated through the cross product method (Schwartz, 1998). For each discontinuity, we automatically calculate the discontinuity thickness by fitting them with a Harris current sheet (discontinuities that are too complicated to be fitted are removed).

Whenever the angle between the magnetic field and the bow shock normal (using the Merka et al. (2005) model scaled to the MMS position with ion bulk velocity, density, and magnetic field from MMS as input), θ_{Bn}, is less than 60° either before or after the discontinuity, we calculate the ambient foreshock ion parameters (density, thermal speed, and parallel speed) by removing the solar wind ions from the ion distributions (see detailed method in Liu et al. (2017) and Liu et al. (2022b)). Due to the uncertainty of model bow shock normal and thus θ_{Bn}, some pristine solar wind time could be included, and sometimes the foreshock ion density is too low causing the calculated foreshock ion parameters to be dominated by noises. Therefore, the calculated foreshock ion density is required to be more than 0.05 cm^{-3} based on a statistical test in Liu et al. (2022b) about whether the calculated density shows a reasonable dependence on the distance to the model bow shock. We thus obtain enough parameters to calculate Eq. (2) on the side of the discontinuity where $\theta_{Bn} < 60°$ (so when both sides have $\theta_{Bn} < 60°$, there can be two model values for one discontinuity). If the negative peak of $j(x)$ is stronger than the positive peak, we then calculate Eq. (3), the transient expansion speed, as shown in Figure 2c. The discontinuity list can be found in the supporting information.

Because the expansion of solar wind plasma can pile up magnetic field and density and deviate velocity direction, it is expected that faster expansion should be associated with stronger magnetic field disturbances and dynamic pressure disturbances. We thus test the model with the observed disturbances. For each discontinuity, we measured the minimum and maximum field strengths within 1 min and the variance and mean values of the field strengths within 5 min from MMS. As introduced in Section 2, our model can only describe the disturbances by foreshock ions at nearly pristine discontinuities, but the PVI method can also automatically identify significant foreshock disturbances like SLAMS (see review by Wilson, 2016), HFAs, and FBs. To remove them, we set a criterion that the variance relative to the mean field strength should be less than 0.15 based on some case studies. We also require that the maximum and minimum field strengths relative to the mean field strength should be larger than the variance, otherwise the disturbances could just be background waves. Like for the field strengths, we also calculate the dynamic pressure variations around the discontinuities along the GSE-X direction and along the local bow shock normal direction (using the Merka et al. (2005) model) using total ion bulk velocity and density measured by MMS.

In summary, we first use magnetic fields measured by MMS to automatically identify discontinuities using the PVI method whenever MMS was in the upstream region. For each discontinuity, we calculate the model values using foreshock ion moments after the removal of solar wind ions from ion distribution functions measured by MMS. We then examine the correlation between the model values and the disturbances of magnetic field strengths and total ion dynamic pressures locally measured by MMS at each discontinuity.

We also conduct case studies for fully formed HFAs and FBs, because maybe large model expansion speeds during early formation stage favor further evolution into significant foreshock transients. To observe the pristine discontinuities that drive those HFAs and FBs, we use the two probes of the Acceleration Reconnection Turbulence & Electrodynamics of Moon's Interaction with the Sun (ARTEMIS) mission (Angelopoulos, 2010), a spin-off of the THEMIS mission, in conjunction with MMS observations. We measure the solar wind ion moments using the THEMIS electrostatic analyzer (ESA) (McFadden et al., 2008) and the IMF using the THEMIS fluxgate magnetometer (Auster et al., 2008). Using the HFA/FB event list in Liu et al. (2022) and requiring ARTEMIS to be in the Fast Survey (high-time resolution) mode during its conjunction with MMS, we select 9 events for case studies (Table 1). We use ARTEMIS to calculate the discontinuity and solar wind parameters and use MMS to measure the ambient foreshock ion parameters to calculate the model for each HFA/FB.

4. Model vs. Observations

In Figure 3a, the upper (lower) half of the plot shows the comparison between the model expansion speeds and the measured maximum (minimum) field strength normalized to the background field strength. There are ~1000 events in this plot. There is a moderate correlation that larger model values tend to be associated with stronger field strength increases (decreases) at the upper (lower) half, with absolute Pearson correlation coefficient of 0.55 (0.51). In the lower half of the plot, there are many scattered dots indicating very significant field strength decreases (and thus weaker correlation than the upper half), partly because many solar wind discontinuities are naturally associated with low field strengths regardless of foreshock ions.

To examine whether the correlation in Figure 3a may be obtained simply because more foreshock ions cause stronger disturbances, Figure 3b compares the field strength disturbances with the density ratio of foreshock ions to solar wind ions. There is a similar trend as in Figure 3a except that the correlation is weak (absolute correlation coefficients ~ 0.3 – 0.5). Figure 3c shows the comparison after the density ratio is removed from the model. We see that the similar trend remains, and the correlation coefficients are weaker or comparable to those in Figure 3b. Therefore, our model of the foreshock ion – discontinuity interaction, which was derived by calculating the foreshock ion gyrovelocity within discontinuities, indeed captures more of the physics than simply the density ratio, because it correlates better with the observations of the magnetic field strength increases and decreases.

Figures 4a-e show the comparison with all the other parameters involved in the model. All of them exhibits a very weak correlation (absolute correlation coefficients ~0.1 – 0.3). There are only very weak trends suggestive that perhaps very large foreshock ion thermal speeds (Figure 4b), very thin discontinuities (Figure 4d), and very low field strengths (Figure 4e) may favor large field strength variation. (And together, these quantities may indicate a large foreshock ion gyroradius relative to the discontinuity thickness, which is already physically described in Eq. (2)). These results suggest that our model can combine many parameters that show a very weak or weak correlation with field strength variation in such a physically justified function that has a moderate correlation (absolute correlation coefficients slightly larger than 0.5) with the field strength change. Figure 4f checks the model expansion speed normalized to the Alfvén speed against the data in the same way. It too shows that the model expansion Mach number does not have a better correlation than that in Figure 3a. Testing the solar wind speed and density, we also find that they do not show any correlations with the field strength variations either (not shown). In sum, our model shows the strongest correlation coefficients among all the tested parameters.

Figure 5 compares the model expansion speeds with the solar wind dynamic pressure disturbances along the GSE-X direction. There is a very weak correlation with the dynamic pressure increases but there is a moderate correlation with the dynamic pressure decreases with an absolute correlation coefficient greater than 0.5. Because a flow deflection only decreases the dynamic pressure while a density variation leads to both, it is reasonable to see a clearer dynamic pressure decrease than increase. Because some events are around the bow shock flank, Figure S1 compares the solar wind dynamic pressure disturbances along the local bow shock normal direction (using the Merka et al. (2005) model), which shows similar results as Figure 5.

Figure 5 suggests that our model can potentially be used to predict the significance of dynamic pressure disturbances driven by the foreshock ion-discontinuity interaction. For example, when the model value is large, e.g., larger than 10, there will be high probability of strong dynamic pressure decreases by more than 20%. When the model value is intermediate, e.g., 3 to 10, the dynamic pressure decreases are mostly around 20%. When the model value is small, e.g., below 3, the dynamic pressure decreases are mostly below 20% and negligible.

To further examine this, we applied case studies using ARTEMIS to observe the pristine discontinuities and MMS to observe the foreshock ion properties around HFAs/FBs that already show significant dynamic pressure disturbances. Table 1 shows the observed foreshock ion and discontinuity parameters and the calculated expansion speed for 9 events. Their model expansion speeds are mostly around and above 10. However, a large model value does not necessarily denote the presence of an HFA or FB. For example, in Figure 2 at ~15:20-15:30 UT, the model value is above 10 and there is indeed a significant dynamic pressure decrease (first vertical shaded region in Figure 2g). However, the density decrease is not significant, which may not satisfy the criteria of HFAs or FBs. Similarly, at ~15:50-16:00 UT, the density depletion is large resulting in a strong dynamic pressure decrease (second vertical shaded region in Figure 2g), but the deflection is weak. Nevertheless, we do not have to predict the presence of HFAs or FBs if we can directly predict the dynamic pressure disturbances (one important input of space weather models). We will further discuss this in Section 5.

Naturally, our model cannot describe all the foreshock disturbances, as we only considered here the scenario of a localized foreshock ion interaction with a single discontinuity. For example, at 15:40-15:50 UT in Figure 2, there is a foreshock cavity (e.g., Sibeck et al., 2002; Omidi et al., 2013a) or traveling foreshock (Kajdič et al., 2017) with a large-scale low dynamic pressure region compared to the ambient solar wind, which is not described by our model. Additionally, other types of foreshock transients, like spontaneous hot flow anomalies (Omidi et al., 2013b; Zhang et al., 2013) that are not associated with solar wind discontinuities, also cannot be described by our model. More effort will be needed in the future to fully model these complex or alternate types of foreshock disturbances.

When calculating the model, we required that the negative peak of $j(x)$ should be stronger than the positive peak to ensure that the direction of foreshock ion-driven current decreases field strengths at discontinuities in order to sustain the expansion. To test whether this requirement is necessary, Figure 6 shows the comparison when we set up an opposite requirement. We see that the correlation to both the field strength disturbances and dynamic pressure disturbances is very weak with absolute correlation coefficients smaller than 0.3. But there is still a trend, since foreshock ion-driven current in the opposite direction should still be able to cause some disturbances, but we do not expect them to develop into significant HFAs or FBs. Local hybrid simulations are needed to further investigate this. Overall, Figure 6 indicates that our requirement of $j(x)$ direction is necessary to enhance the model performance.

One reason for our interest in predicting HFAs and FBs is to forecast their significant dynamic pressure depletions. However, the identification criteria of HFAs and FBs in observations are mostly empirical (e.g., density depletion, field strength depletion, and flow deflection by a certain percent). As a result, even if the foreshock ion-discontinuity interaction can result in strong dynamic pressure disturbances, they may not be strong enough to result in an HFA or FB immediately. For example, when an HFA or FB just starts to form, it is in an intermediate stage of evolution that may not meet all the selection criteria. These transients may also not be able to finish the formation, e.g., because the background ULF waves disturbed the needed background environment, or the driver discontinuity has convected out of the foreshock. Or they can finish the formation, but the ambient foreshock ion parameters are not strong enough to ensure the formed structures satisfy all the criteria. (Such structures are categorized as density holes by Lu et al. (2022).) Therefore, it is more practical and efficient to directly predict whether there will be dynamic pressure disturbances than predict whether there will be a well-defined HFA or FB.

Table 1. The density ratio of foreshock ions to solar wind ions, foreshock ion thermal speed, parallel speed relative to the solar wind, discontinuity shear angle, thickness, IMF strength, and the calculated model value using Eq. (3) of 9 case study events. Based on whether they have two compressional boundaries or only an upstream shock, we categorize them as an HFA-like or FB-like event. Because when the foreshock ion density is low, it can be affected by the 1-count noise (~0.0075 cm^{-3} calculated during non-foreshock time), we thus include the uncertainty of foreshock ion density ratio (dn ratio).

Time (UT)	Type	n ratio	dn ratio	Vth [km/s]	Vpara [km/s]	Shear [°]	Thickness [km]	Bt [nT]	Model [km/s]
2017-12-18/12:01	FB	0.1	0.003	750	-998	35.6	1641	2.7	37
2017-12-18/12:09	HFA	0.24	0.003	612	-965	44.8	30259	3.1	31
2017-12-18/12:56	FB	0.087	0.003	622	-1056	26.9	1319	2.8	25
2017-12-18/13:58	HFA	0.077	0.003	758	-611	22.6	666	3.2	17
2017-12-18/14:11	HFA	0.031	0.003	970	-737	20.7	3322	3.3	8
2018-01-12/01:51	FB	0.034	0.001	524	-524	93.8	1401	2.6	11
2018-12-10/05:48	HFA	0.043	0.003	920	456	22	6954	4.1	8
2018-12-10/07:45	HFA	0.08	0.003	838	193	-61	3147	3.7	20
2019-01-08/01:47	FB	0.035	0.001	719	422	-63.9	733	2.9	14

5. Summary and Discussion

In summary, we evaluate the efficacy of a quantitative model describing the expansion speed of foreshock transients driven by foreshock ion interaction with a solar wind discontinuity. We find that the model is consistent with local hybrid simulations. Comparing the model with a statistical database of observations, we find a moderate correlation between model predictions and data for the field strength variations and the dynamic pressure decreases around discontinuities. This correlation (absolute correlation coefficients >0.5) is better than the correlation between all other possible observed parameters and the above data quantities. Through case studies, we show that numerous fully formed HFAs and FBs are typically associated with large model expansion speed values. Our results suggest that given foreshock ion parameters at specific bow shock positions and solar wind discontinuity parameters (e.g., at lunar distance or at L1), the proposed model can predict with reasonable success probability the field strength variations and dynamic pressure decreases driven by foreshock ion – discontinuity interactions.

Next, we discuss the limitations and possible future improvements of our model. (1) The model only considers the motion of foreshock ions arriving from only one side of the discontinuity. When a discontinuity is embedded within the foreshock, the interaction of foreshock ions arriving from both sides should be considered and compared with local hybrid simulations. (2) What could happen when the foreshock ion-driven current has an unfavorable direction requires further studies. For example, a foreshock compressional boundary may form, which could still result in some disturbances. (3) Our model assumes a stable background field. But in the foreshock, there is typically significant wave activity. How these waves might affect the foreshock ion – discontinuity interaction, including the possibility of suppressing the transient expansion by potentially decorrelating the gyromotion of the ions, should be further studied. (4) Our model assumes constant background foreshock ion parameters, but in reality they are a function of space and time. The model may need to be modified into the form of integral. (5) Even if after including the time dependence into our model (~Δt^2 based on Vu et al. (2023)), we cannot compare the model with observations, because it is extremely difficult for observations to determine when the interaction starts to occur. Global hybrid simulations may help. (6) We assume foreshock ions are field aligned and follow Maxwellian distributions, but foreshock ions can also be ring distributions or gyrophase bunched. These effects complicate the analytical treatment and may invalidate some of our results but need to be considered, at least numerically. (7) The foreshock ion parameters are not yet predictable. Foreshock ion models should be established in the future, in order to provide the necessary input to model foreshock transient formation and evolution.

Because previous studies have established a large database of HFAs and FBs as a function of various upstream conditions, including both observations (e.g., Schwartz et al., 2000; Facskó et al., 2008, 2009, 2010; Chu et al., 2017; Liu et al., 2017, 2022b; Vu et al., 2022b) and simulations (e.g., Omidi et al., 2020; Vu et al., 2023), it could be possible to also establish data-based models, e.g., by training a machine learning model using above database. It is also feasible to combine the physics-based equations and the database to improve the efficiency and accuracy of the model training.

Acknowledgements

T. Z. L. acknowledges the ISSI team, Foreshocks Across The Heliosphere: System Specific Or Universal Physical Processes? led by H. Hietala & F. Plaschke for the meaningful discussion. T. Z. L. is partially supported by NSF award AGS-1941012/2210319, NASA grant 80NSSC21K1437/80NSSC22K0791, and NASA grant 80NSSC23K0086. H. Z. is partially supported by NSF AGS-1352669 and NASA grant 80NSSC18K1376. We acknowledge the NASA THEMIS contract NAS5-02099, the SPEDAS team and NASA's Coordinated Data Analysis Web.

Data availability

MMS data are available at MMS Science Data Center (https://lasp.colorado.edu/mms/sdc/). THEMIS dataset are available at NASA's Coordinated Data Analysis Web (CDAWeb, http://cdaweb.gsfc.nasa.gov/). The SPEDAS software (see Angelopoulos et al. (2019)) is available at http://themis.ssl.berkeley.edu. The discontinuity list is in the supporting information.

Figures

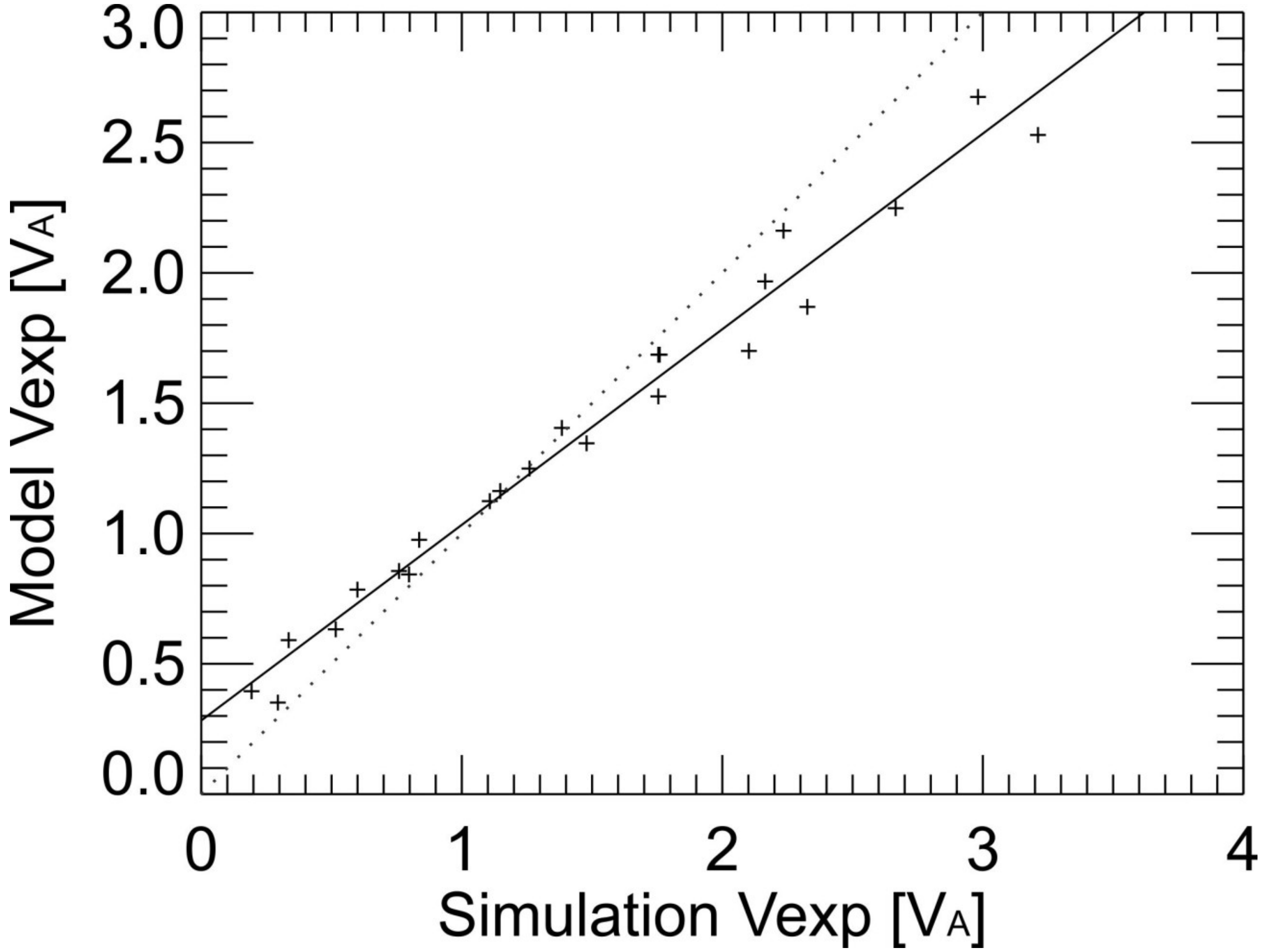

Figure 1. The comparison between the model expansion speeds calculated using Eq. (3) and the measured expansion speeds from the local hybrid simulations using varying foreshock ion parallel speed, thermal speed, and density ratio relative to the solar wind (Vu et al., 2023). The expansion speeds are normalized to the Alfvén speed (V_A). The solid line indicates the linear fitting, and the dotted line indicates the diagonal.

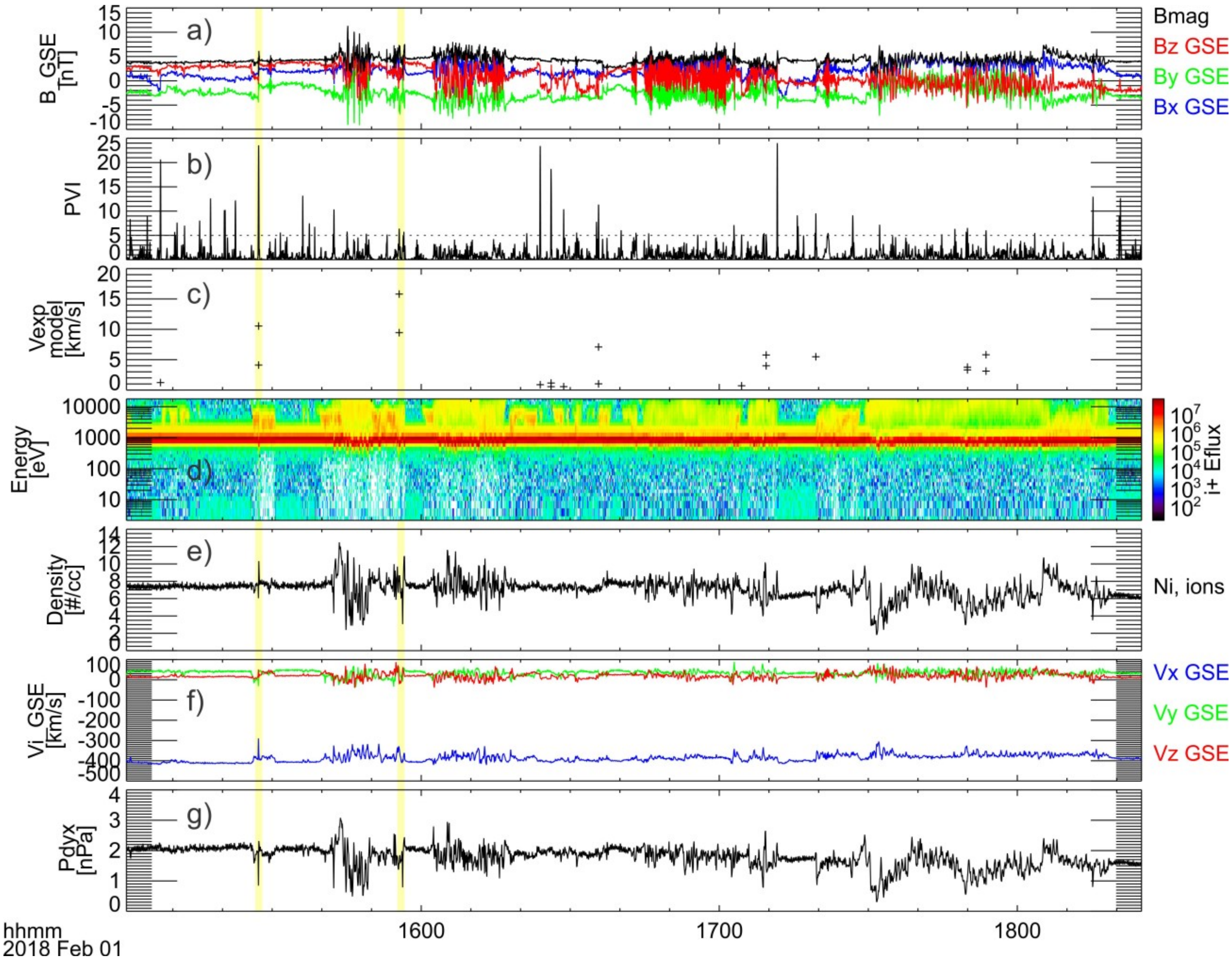

Figure 2. An example time interval demonstrating the statistical study analysis. From top to bottom: (a) magnetic field, (b) PVI (horizontal dotted line indicate the threshold), (c) the model expansion speeds using Eq. (3), (d) ion energy spectrum, (e) ion density, (f) ion bulk velocity, (g) dynamic pressure along GSE-X. The two yellow shaded regions indicate the dynamic pressure decreases associated with large model values.

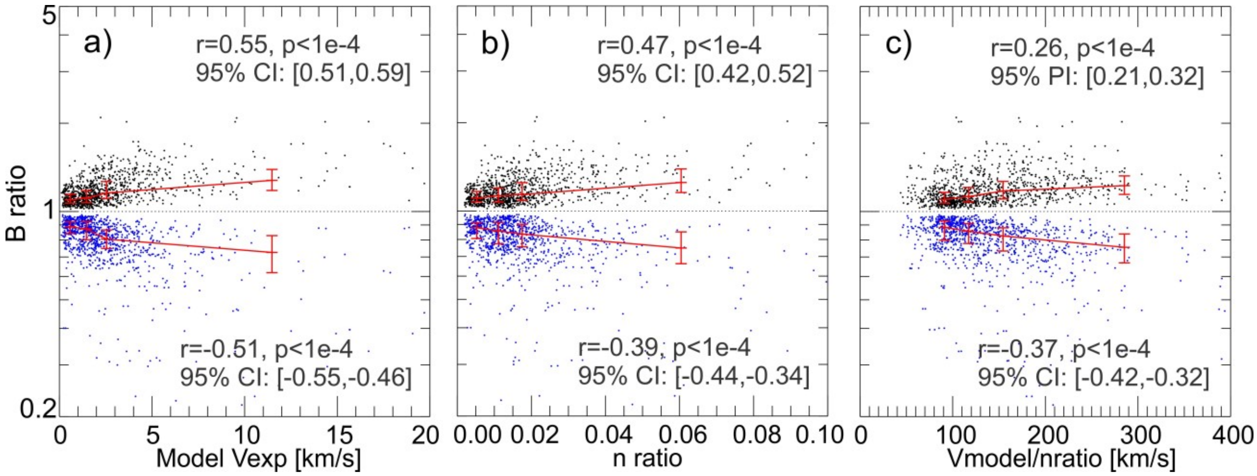

Figure 3. (a) The model expansion speeds vs. the maximum (upper half) and minimum (lower half) field strength normalized to the background field strength. (b) and (c) are in the same format as (a) except that the horizontal axis is the density ratio of foreshock ions to solar wind ions and the model values divided by the density ratio, respectively. The Pearson correlation coefficients (r), p-values (p) calculated from t-tests, and 95% confidence intervals (CI) calculated from Fisher transformation are shown in each panel. Red bars indicate the median values, lower quartiles, and upper quartiles, with event number equally distributed.

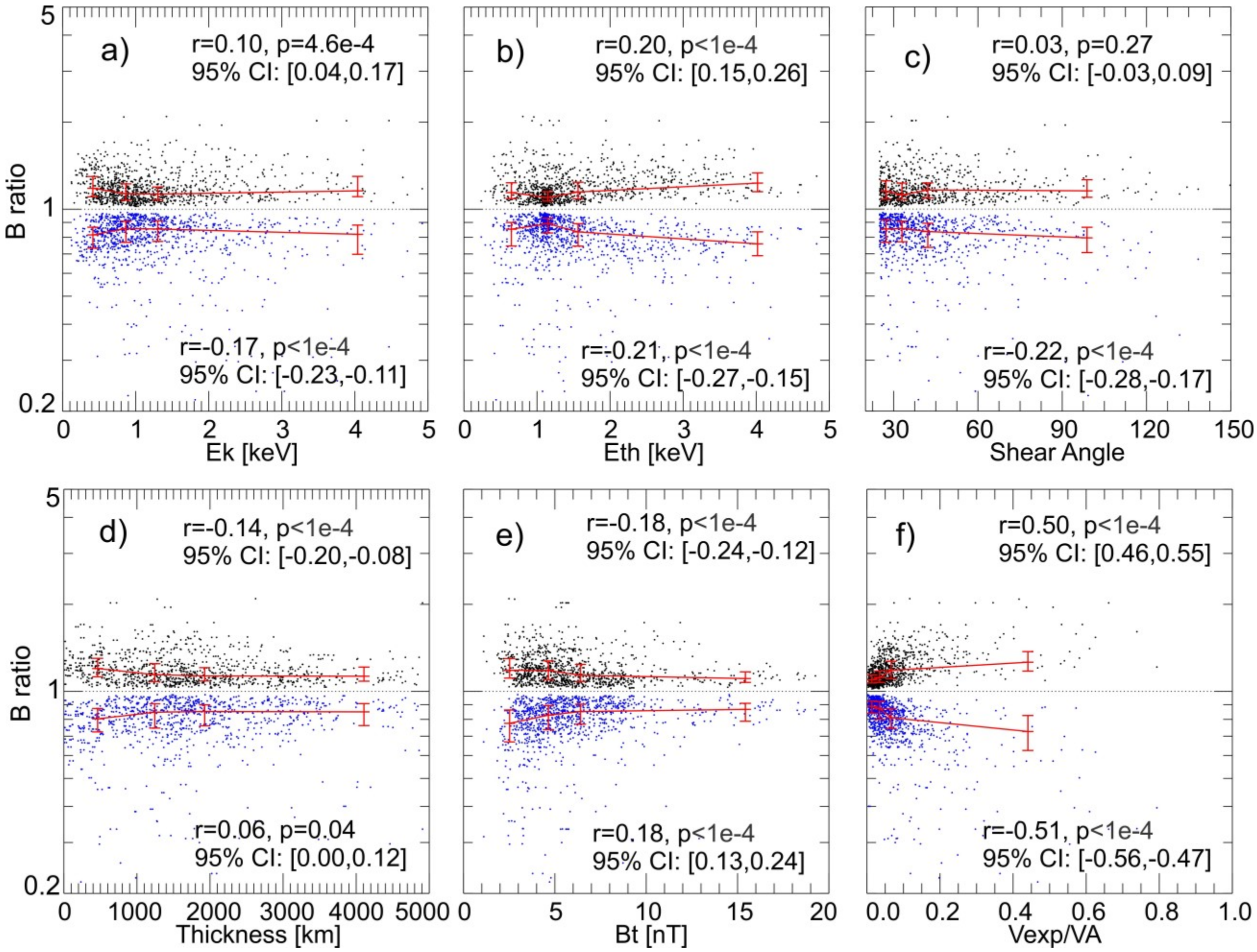

Figure 4. The same format as Figure 3 except that the horizontal axis is (a) the foreshock ion kinetic energy relative to the solar wind, (b) foreshock ion thermal energy, (c) discontinuity shear angle, (d) discontinuity thickness, (e) magnetic field strength, and (f) the model expansion speed normalized to the Alfvén speed.

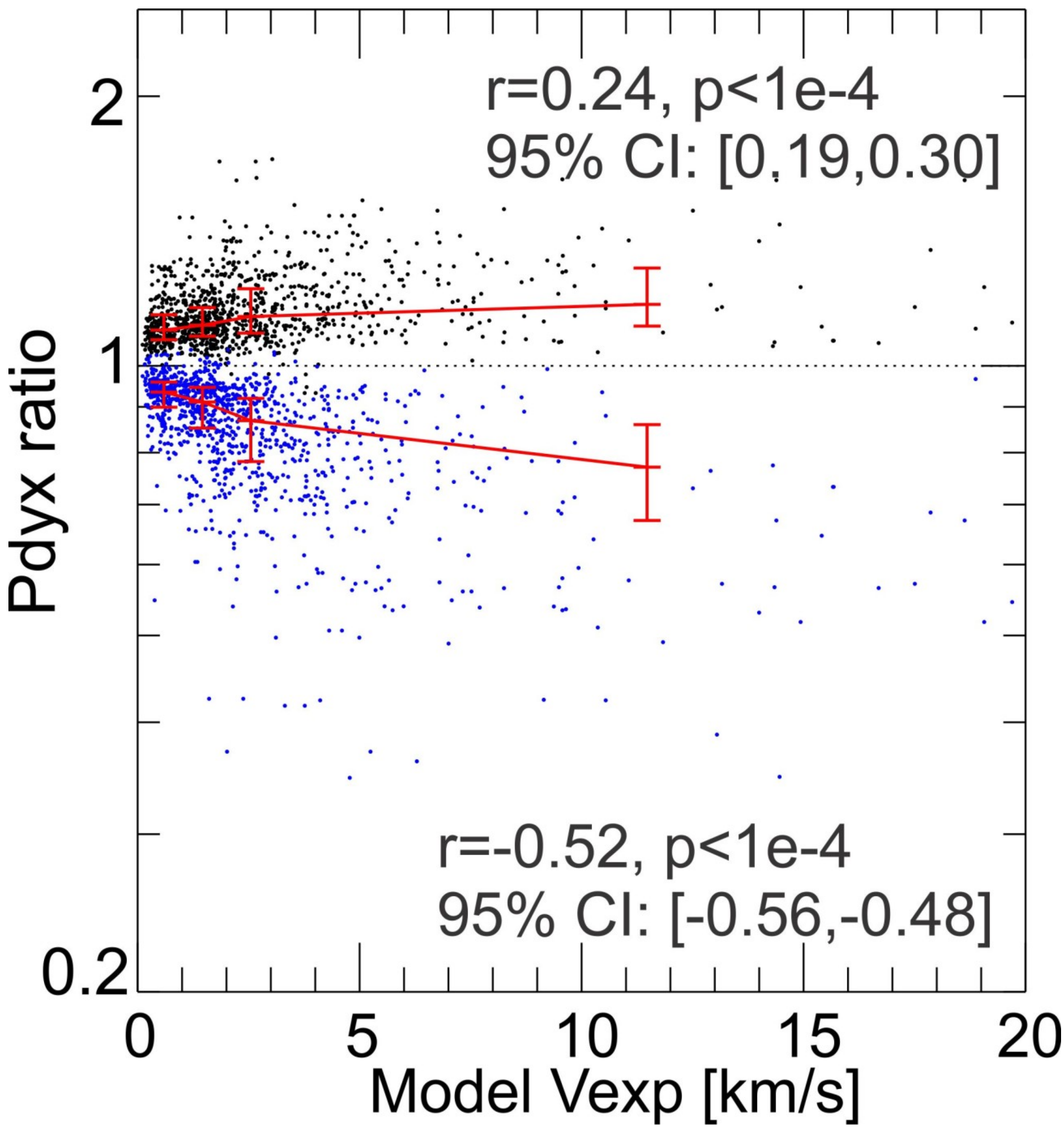

Figure 5. The model expansion speeds vs. the maximum (upper half) and minimum (lower half) dynamic pressure along GSE-X normalized to the background.

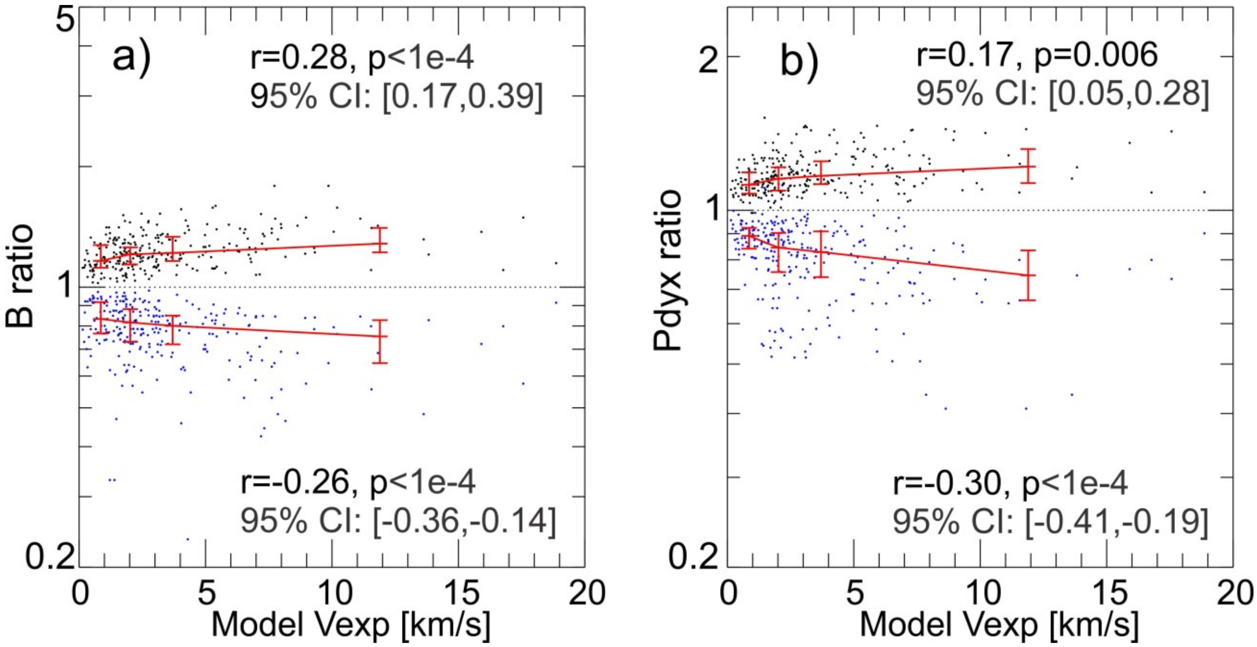

Figure 6. Same format as Figure 3a and Figure 5, except that the model is calculated when the foreshock ion-driven current direction is in an unfavorable way ($j(x) > 0$).

References

An, X., T. Z. Liu, J. Bortnik, A. Osmane, V. Angelopoulos (2020). Formation of foreshock transients and associated secondary shocks. ApJ, 901:73 (16pp), https://doi.org/10.3847/1538-4357/abaf03

Angelopoulos, V. (2010). The ARTEMIS Mission. In: Russell, C., Angelopoulos, V. (eds) The ARTEMIS Mission. Springer, New York, NY. https://doi.org/10.1007/978-1-4614-9554-3_2

Angelopoulos, V., Cruce, P., Drozdov, A. et al. Space Sci Rev (2019) 215: 9. https://doi.org/10.1007/s11214-018-0576-4

Archer, M. O., Turner, D. L., Eastwood, J. P., Horbury, T. S., & Schwartz, S. J. (2014). The role of pressure gradients in driving sunward magnetosheath flows and magnetopause motion. Journal of Geophysical Research: Space Physics, 119, 8117–8125. https://doi.org/10.1002/2014JA020342

Archer, M. O., D. L. Turner, J. P. Eastwood, S. J. Schwartz, and T. S. Horbury (2015), Global impacts of a foreshock bubble: Magnetosheath, magnetopause and ground-based observations, Planet. Space Sci., 106, 56–66, doi:10.1016/j.pss.2014.11.026.

Auster, H. U., et al. (2008), The THEMIS fluxgate magnetometer, Space Sci. Rev., 141, 235–264, doi:10.1007/s11214-008-9365-9.

Burch, J. L., Moore, T. E., Torbert, R. B., & Giles, B. L. (2016). Magnetospheric multiscale overview and science objectives. Space Science Reviews, 199(1 - 4), 5 – 21. https://doi.org/10.1007/s11214-015-0164-9

Burgess, D. (1989). On the effect of a tangential discontinuity on ions specularly reflected at an oblique shock. Journal of Geophysical Research, 94, 472–478. https://doi.org/10.1029/JA094iA01p00472

Burgess, D., E. Möbius, M. Scholer (2012), Ion acceleration at the Earth’s bow shock. Space Sci. Rev. 173(1–4), 5–47. doi:10.1007/s11214-012-9901-5

Chu, C., H. Zhang, D. Sibeck, A. Otto, Q. Zong, N. Omidi, J. P. McFadden, D. Fruehauff, and V. Angelopoulos (2017), THEMIS satellite observations of hot flow anomalies at Earth’s bow shock, Ann. Geophys., 35, 3, 443–451, doi:10.5194/angeo-35-443-2017.

Eastwood, J. P., E. A. Lucek, C. Mazelle, K. Meziane, Y. Narita, J. Pickett, and R. A. Treumann (2005), The Foreshock, Space. Sci. Rev., 118, 41–94, https://doi.org/10.1007/s11214-005-3824-3.

Eastwood, J., Schwartz, S., Horbury, T., Carr, C., Glassmeier, K.-H., Richter, I., et al. (2011). Transient Pc3 wave activity generated by a hot flow anomaly: Cluster, Rosetta, and ground-based observations. Journal of Geophysical Research, 116, A08224. https://doi.org/10.1029/2011JA016467

Facskó, G., Kecskem´ety, K., Erd˝os, G., T´atrallyay, M., Daly, P. W., and Dandouras, I.: A statistical study of hot flow anomalies using Cluster data, Advances in Space Research, 41, 1286–1291, doi: 10.1016/j.asr.2008.02.005, 2008.

Facskó, G., J.G. Trotignon, I. Dandouras, E.A. Lucek, P.W. Daly, Study of hot flow anomalies using Cluster multi-spacecraft measurements, Advances in Space Research, 10.1016/j.asr.2009.08.011, 45, 4, (541-552), (2010).

Facskó, G.; Opitz, A.; Lavraud, B.; Luhmann, J. G.; Russell, C. T.; Sauvaud, J. -A.; Fedorov, A.; Kis, A.; Wesztergom, V., Hot flow anomaly remnant in the far geotail?, Journal of Atmospheric and Solar-Terrestrial Physics, Volume 124, p. 39-43., 2015, doi:10.1016/j.jastp.2015.01.011

Facskó, G.; Nemeth, Z.; Erdos, G.; Kis, A.; Dandouras, I., A global study of hot flow anomalies using Cluster multi-spacecraft measurements, Annales Geophysicae, Volume 27, Issue 5, 2009, pp.2057-2076, 2009, doi:10.5194/angeo-27-2057-2009

Fillingim, M. O., Eastwood, J. P., Parks, G. K., Angelopoulos, V., Mann, I. R., Mende, S. B., & Weatherwax, A. T. (2011). Polar UVI and THEMIS GMAG observations of the ionospheric response to a hot flow anomaly. Journal of Atmospheric and Solar-Terrestrial Physics, 73(1), 137–145. https://doi.org/10.1016/j.jastp.2010.03.001

Kajdič, P., Blanco-Cano, X., Omidi, N., Rojas-Castillo, D., Sibeck, D. G., & Billingham, L. (2017). Traveling foreshocks and transient foreshock phenomena. Journal Geophysical Research: Space Physics, 122, 9148– 9168, https://doi.org/10.1002/2017JA023901

Greco, A., Chuychai, P., Matthaeus, W. H., Servidio, S., & Dmitruk, P. (2008). Intermittent MHD structures and classical discontinuities. Geophysical Research Letters. https://doi.org/10.1029/2008GL035454

Hartinger, M. D., D. L. Turner, F. Plaschke, V. Angelopoulos, and H. Singer (2013), The role of transient ion foreshock phenomena in driving Pc5 ULF wave activity, J. Geophys. Res. Space Physics, 118, doi:10.1029/2012JA018349.

Lee, S. H., Sibeck, D. G., Omidi, N., Silveira, M. V. D., Giles, B. L., Torbert, R. B., et al. (2021). Comparison of MMS observations of foreshock bubbles with a global hybrid simulation. Journal of Geophysical Research: Space Physics, 126, e2020JA028848. https://doi.org/10.1029/2020JA028848

Lin, Y. (1997), Generation of anomalous flows near the bow shock by its interaction with interplanetary discontinuities, J. Geophys. Res., 102 (A11), 24265– 24281, doi:10.1029/97JA01989.

Lin, Y. (2002), Global hybrid simulation of hot flow anomalies near the bow shock and in the magnetosheath, Planetary and Space Science, 50, 577 – 591

Liu, Z., Turner, D. L., Angelopoulos, V., & Omidi, N. (2015). THEMIS observations of tangential discontinuity-driven foreshock bubbles. Geophysical Research Letters, 42, 7860–7866. https://doi.org/10.1002/2015GL065842

Liu, T. Z., D. L. Turner, V. Angelopoulos, and N. Omidi (2016), Multipoint observations of the structure and evolution of foreshock bubbles and their relation to hot flow anomalies, J. Geophys. Res. Space Physics, 121, doi:10.1002/2016JA022461.

Liu, T. Z., Angelopoulos, V., Hietala, H., & Wilson, L. B. III (2017). Statistical study of particle acceleration in the core of foreshock transients. Journal of Geophysical Research: Space Physics, 122, 7197–7208. https://doi.org/10.1002/2017JA024043

Liu, T. Z., Wang, C.-P., Wang, B., Wang, X., Zhang, H., Lin, Y., et al. (2020a). ARTEMIS observations of foreshock transients in the midtail foreshock. Geophysical Research Letters, 47, e2020GL090393. https://doi.org/10.1029/2020GL090393

Liu, T. Z., X. An, H. Zhang, and D. Turner (2020b), Magnetospheric Multiscale (MMS) observations of foreshock transients at their very early stage, ApJ, 902:5 (15pp), https://doi.org/10.3847/1538-4357/abb249

Liu, T. Z., Zhang, H., Wang, C.-P., Angelopoulos, V., Vu, A., Wang, X., & Lin, Y. (2021). Statistical study of foreshock transients in the midtail foreshock. Journal of Geophysical Research: Space Physics, 126, e2021JA029156. https://doi.org/10.1029/2021JA029156

Liu, T. Z., Wang, C.-P., Wang, X., Angelopoulos, V., Zhang, H., Lu, X., & Lin, Y. (2022a). Magnetospheric field-aligned current generation by foreshock transients: Contribution by flow vortices and pressure gradients. Journal of Geophysical Research: Space Physics, 127, e2022JA030700. https://doi.org/10.1029/2022JA030700

Liu, T. Z., H. Zhang, D. Turner, A. Vu, and V. Angelopoulos (2022b). Statistical study of favorable foreshock ion properties for the formation of hot flow anomalies and foreshock bubbles, Journal of Geophysical Research: Space Physics, 127, e2022JA030273. https://doi.org/10.1029/2022JA030273

Liu, T. Z., A. Vu, H. Zhang, X. An, and V. Angelopoulos (2023). Predictive expansion speed model for foreshock bubbles. Journal of Geophysical Research: Space Physics, 128, e2022JA030814. https://doi.org/10.1029/2022JA030814

Liu, T. Z., V. Angelopoulos, A. Vu, and H. Zhang (2022). Foreshock ion motion across discontinuities: formation of foreshock transients. Submitted to JGR.

Lu, X., Zhang, H., Liu, T., Vu, A., Pollock, C., & Wang, B. (2022). Statistical study of foreshock density holes. Journal of Geophysical Research: Space Physics, 127, e2021JA029981. https://doi.org/10.1029/2021JA029981

Lucek, E. A., Horbury, T. S., Balogh, A., Dandouras, I., and Rème, H. (2004), Cluster observations of hot flow anomalies, J. Geophys. Res., 109, A06207, doi:10.1029/2003JA010016.

McFadden, J. P., C. W. Carlson, D. Larson, V. Angelopoulos, M. Ludlam, R. Abiad, B. Elliott, P. Turin, and M. Marckwordt (2008), The THEMIS ESA plasma instrument and in-flight calibration, Space Sci Rev., 141, 277–302, doi:10.1007/s11214-008-9440-2.

Merka, J., A. Szabo, J. A. Slavin, and M. Peredo (2005), Three-dimensional position and shape of the bow shock and their variation with upstream Mach numbers and interplanetary magnetic field orientation, J. Geophys. Res., 110 A04202, doi:10.1029/2004JA010944.

Omidi, N. and D. G. Sibeck (2007), Formation of hot flow anomalies and solitary shocks, J. Geophys. Res., 112, A10203, doi:10.1029/2006JA011663.

Omidi, N., J. P. Eastwood, and D. G. Sibeck (2010), Foreshock bubbles and their global magnetospheric impacts, J. Geophys. Res., 115, A06204, doi:10.1029/2009JA014828.

Omidi, N., Sibeck, D., Blanco-Cano, X., Rojas-Castillo, D, Turner, D., Zhang, H., and Kajdič, P. (2013a), Dynamics of the foreshock compressional boundary and its connection to foreshock cavities, J. Geophys. Res. Space Physics, 118, 823– 831, doi:10.1002/jgra.50146.

Omidi, N., H. Zhang, D. Sibeck, and D. Turner (2013b), Spontaneous hot flow anomalies at quasi-parallel shocks: 2. Hybrid simulations, J. Geophys. Res., VOL. 118, 173–180, doi:10.1029/2012JA018099.

Omidi, N., Lee, S. H., Sibeck, D. G., Turner, D. L., Liu, T. Z., & Angelopoulos, V. (2020). Formation and topology of foreshock bubbles. Journal of Geophysical Research: Space Physics, 125, e2020JA028058. https:// doi.org/10.1029/2020JA028058

Pollock, C., Moore, T., Jacques, A., Burch, J., Gliese, U., Saito, Y., et al. (2016). Fast plasma investigation for magnetospheric multiscale. Space Science Reviews, 199(1 - 4), 331 – 406. https://doi.org/10.1007/s11214-016-0245-4

Russell, C. T., Anderson, B. J., Baumjohann, W., Bromund, K. R., Dearborn, D., Fischer, D., et al. (2016). The magnetospheric multiscale magnetometers. Space Science Reviews, 199(1 - 4), 189–256. https://doi.org/10.1007/s11214-014-0057-3

Schwartz, S. J., et al. (1985), An active current sheet in the solar wind, Nature, 318, 269-271.

Schwartz, S. J. (1998), Shock and discontinuity normal, Mach numbers, and related parameters, in Analysis Methods for Multi-Spacecraft Data, ISSI Sci. Rep. SR-001, edited by G. Paschmann and P. W. Daly, pp. 249–270, ISSI/ESA, Noordwijk, Netherlands.

Schwartz, S. J., Paschmann, G., Sckopke, N., Bauer, T. M., Dunlop, M., Fazakerley, A. N., and Thomsen, M. F. (2000), Conditions for the formation of hot flow anomalies at Earth's bow shock, J. Geophys. Res., 105(A6), 12639– 12650, doi:10.1029/1999JA000320.

Schwartz S. J., Avanov, L., Turner, D., Zhang, H., Gingell, I., Eastwood, J. P., et al. (2018). Ion kinetics in a hot flow anomaly: MMS observations. Geophysical Research Letters. 45. https://doi.org/10.1029/2018GL080189

Shen, X.-C., Shi, Q., Wang, B., Zhang, H., Hudson, M. K., Nishimura, Y., et al. (2018). Dayside magnetospheric and ionospheric responses to a foreshock transient on 25 June 2008: 1. FLR observed by satellite and ground-based magnetometers. Journal of Geophysical Research: Space Physics, 123, 6335– 6346. https://doi.org/10.1029/2018JA025349

Shi, F., Y. Lin, and X. Wang (2013), Global hybrid simulation of mode conversion at the dayside magnetopause, J. Geophys. Res. Space Physics, 118, 6176–6187, doi:10.1002/jgra.50587.

Shi, F., Cheng, L., Lin, Y., and Wang, X. (2017), Foreshock wave interaction with the magnetopause: Signatures of mode conversion, J. Geophys. Res. Space Physics, 122, 7057– 7076, doi:10.1002/2016JA023114.

Shi, X., Hartinger, M. D., Baker, J. B. H., Ruohoniemi, J. M., Lin, D., Xu, Z., et al. (2020). Multipoint conjugate observations of dayside ULF waves during an extended period of radial IMF. Journal of Geophysical Research: Space Physics, 125, e2020JA028364. https://doi.org/10.1029/2020JA028364

Sibeck, D. G., et al. (1999), Comprehensive study of the magnetospheric response to a hot flow anomaly, J. Geophys. Res., 104(A3), 4577–4593, doi:10.1029/1998JA900021.

Thomas, V. A., Winske, D., Thomsen, M. F., and Onsager, T. G. (1991), Hybrid simulation of the formation of a hot flow anomaly, J. Geophys. Res., 96(A7), 11625– 11632, doi:10.1029/91JA01092.

Turner D. L., N. Omidi, D. G. Sibeck, and V. Angelopoulos (2013), First observations of foreshock bubbles upstream of Earth’s bow shock: Characteristics and comparisons to HFAs, J. Geophys. Res., VOL. 118, 1552–1570, doi:10.1002/jgra.50198.

Turner, D. L., Liu, T. Z., Wilson, L. B., Cohen, I. J., Gershman, D. G., Fennell, J. F., et al (2020). Microscopic, multipoint characterization of foreshock bubbles with Magnetospheric Multiscale (MMS). Journal of Geophysical Research: Space Physics, 125, e2019JA027707. https://doi.org/10.1029/2019JA027707

Vu, A., Liu, T., Zhang, H., Delamere, P. (2022a). Hybrid Simulations of a Tangential Discontinuity-Driven Foreshock Bubble Formation in Comparison with a Hot Flow Anomaly Formation, Journal of Geophysical Research: Space Physics, 127, e2021JA029973, DOI: 10.1029/2021JA029973

Vu, A., Liu, T. Z., Zhang, H., & Pollock, C. (2022b). Statistical Study of Foreshock Bubbles, Hot Flow Anomalies, and Spontaneous Hot Flow Anomalies and their Substructures Observed by MMS. Journal of Geophysical Research: Space Physics, 127, e2021JA030029. https://doi.org/10.1029/2021JA030029

Vu, A., Liu, T., Zhang, H., Delamere, P. (2023). Parameter Dependencies of Early-Stage Tangential Discontinuity-Driven Foreshock Bubbles in Local Hybrid Simulations. Journal of Geophysical Research: Space Physics, 128, e2022JA030815. https://doi.org/10.1029/2022JA030815

Wang, B., Nishimura, Y., Hietala, H., Shen, X.-C., Shi, Q., Zhang, H., et al. (2018). Dayside magnetospheric and ionospheric responses to a foreshock transient on 25 June 2008: 2. 2-D evolution based on dayside auroral imaging. Journal of Geophysical Research: Space Physics, 123, 6347– 6359. https://doi.org/10.1029/2017JA024846

Wang, B., Liu, T., Nishimura, Y., Zhang, H., Hartinger, M., Shi, X., et al. (2020). Global propagation of magnetospheric Pc5 ULF waves driven by foreshock transients. Journal of Geophysical Research: Space Physics, 125, e2020JA028411. https://doi.org/10.1029/2020JA028411

Wang, B., Zhang, H., Liu, Z., Liu, T., Li, X., & Angelopoulos, V. (2021). Energy modulations of magnetospheric ions induced by foreshock transient-driven ultralow-frequency waves. Geophysical Research Letters, 48, e2021GL093913. https://doi.org/10.1029/2021GL093913

Wang, C.-P., Liu, T. Z., Xing, X., & Masson, A. (2018). Multispacecraft observations of tailward propagation of transient foreshock perturbations to midtail magnetosheath. Journal of Geophysical Research: Space Physics, 123, 9381–9394. https://doi.org/10.1029/2018JA025921

Wang, C.-P., Wang, X., Liu, T. Z., & Lin, Y. (2020). Evolution of a foreshock bubble in the midtail foreshock and impact on the magnetopause: 3D global hybrid simulation. Geophysical Research Letters, 47, e2020GL089844. https://doi.org/10.1029/2020GL089844

Wang C-P, Wang X, Liu TZ, and Lin Y (2021a). Impact of Foreshock Transients on the Flank Magnetopause and Magnetosphere and the Ionosphere. Front. Astron. Space Sci. 8:751244. doi: 10.3389/fspas.2021.751244

Wang, C.-P., Wang, X., Liu, T. Z., & Lin, Y. (2021b). A foreshock bubble driven by an IMF tangential discontinuity: 3D global hybrid simulation. Geophysical Research Letters, 48, e2021GL093068. https://doi.org/10.1029/2021GL093068

Wilson, L.B., III (2016). Low Frequency Waves at and Upstream of Collisionless Shocks. In Low-Frequency Waves in Space Plasmas (eds A. Keiling, D.-H. Lee and V. Nakariakov). doi:10.1002/9781119055006.ch16

Zhang, H., et al. (2010), Time history of events and macroscale interactions during substorms observations of a series of hot flow anomaly events, J. Geophys. Res., 115, A12235, doi:10.1029/2009JA015180.

Zhang H., D. G. Sibeck, Q.-G. Zong, N. Omidi, D. Turner, and L. B. N. Clausen (2013), Spontaneous hot flow anomalies at quasi-parallel shocks: 1. Observations, J. Geophys. Res., VOL. 118, 3357–3363, doi:10.1002/jgra.50376

Zhang, H., Zong, Q.-G., Connor, H. et al. Dayside transient phenomena and their impact on the magnetosphere and ionosphere. Space Sci Rev (2022). DOI: 10.1007/s11214-021-00865-0

Zhao, L. L., Zhang, H., and Zong, Q. G. (2017), Global ULF waves generated by a hot flow anomaly, Geophys. Res. Lett., 44, 5283– 5291, doi:10.1002/2017GL073249.